Subpixel Target Detection in Hyperspectral Imaging

François Vincent
University of Toulouse-ISAE
Toulouse, France
Email: francois.vincent@isae.fr

Olivier Besson
University of Toulouse-ISAE
Toulouse, France
Email: olivier.besson@isae.fr

***Abstract*—Detecting a target of known spectral signature from an unknown background is one of main goal of hyperspectral imaging. As the majority of hyperspectral imaging systems have a poor spatial resolution, subpixel targets are usual. In this case, the so-called replacement model is commonly advocated. This model, valid for reflectance images, specifies that if a target is present, the amount of background should reduce in the same proportion. Nevertheless, the majority of the standard detectors, such as the Match Filter or the Kelly detector, have been developed for different contexts, and do not exploit this constraint. One of the rare example that is suitable for the replacement model is the Finite Target Match Filter, which is known to improve the target selectivity detection. In this paper, we develop the exact Generalized Likelihood Ratio Test for the model at hand. We show that this new detector outperforms the standard ones, on a real data experiment.**

I. Introduction

Hyperspectral imaging is the extension of a standard 3-colors picture to a hundred of spectral samples map. Hence, each pixel contains a spectroscopy signature linked to the materials belonging to the area of interest. As a consequence, hyperspectral imaging is becoming a useful tool to deeply analyse the environment in many applications, such as earth observation and remote sensing [1], astronomy [2], defense [3], mine detection [4] [5], gas detection [6], food safety [7], or medicine [8].

One of the main goal of hyperspectral imaging is to detect a target of known signature from an unknown background. Many detection algorithms have been developed, most of them assuming a Gaussian distribution for the background and noise. Among the most popular schemes, we can quote the Matched Filter (MF) [9] or the Constrained Energy Minimization (CEM) [10], that only differ from the presence or not of the signal of interest in the covariance matrix used to whiten the data. The Orthogonal Subspace Projection (OSP) [11] is also a high Signal to Noise Ratio (SNR) approximation of such schemes. Another popular detector offering very good performance especially when the number of secondary data is small, is the Generalized Likelihood Ratio Test (GLRT) developed by Kelly [12]. To complete this short list of the most used detectors, we can mention the Adaptive Coherent/Cosine Estimator (ACE) [13] that considers a possible scaling factor between the Pixel Under Test (PUT) and the secondary pixels. As these algorithms have been derived for third applications, such as radar processing, they are not exactly adapted to hyperspectral reflectance maps. Indeed, the raw radiance measurements recovered at the sensor level are usually transformed in reflectances, to eliminate the effects of the non-uniform sun illumination and atmospheric effects. Thus, the pixel's signatures can be compared to laboratory targets measurements, called endmenbers. This useful pre-processing step can be conducted using atmospheric and sun illumination models, such as $6S$ [14], MODTRAN [15], or EXACT [16], but also, identifying ground targets and comparing them to their known signature. An example of such a technique is the Empirical Line Method (ELM) [15] [17] that estimates the supposed linear relationship between the radiance and the reflectance using a Mean Least Square (MLS) optimization. As a consequence of this pre-processing, the endmembers amplitudes represent the proportion of the corresponding material, called abundance. The standard model used in this case is the so-called Linear Mixing Model (LMM), where the sum of abundances is then constrained to be one. In case of subpixel target, this model is also referred to the replacement model, as when a target is present in the PUT, the background abundance should reduce in the same proportion.

As stated before, most above-cited detectors, which are commonly used for reflectance maps, have been derived for the standard additive model, without any constraint on the vector's amplitudes. One of the rare algorithm developed for the model at hand is the so-called Finite Target Matched Filter (FTMF) [18], which is the adaptation of the MF to the replacement model. If the background is assumed to be Gaussian distributed, it consists in a two-step GLRT, where the mean and covariance matrix of the background are estimated from secondary data. This detector is shown to have a better target selectivity than the standard MF, i.e. it reduces the false alarms due to the presence of close-endmembers targets, by naturally taking into account the target and background abundance [18]. This target selectivity improvement is of utmost importance in geological remote sensing or defence applications when searching for a specific material or target.

In this paper, we derive the exact, i.e. one-step, GLRT for the replacement model. This detector is then the counterpart of the popular Kelly algorithm for the replacement model. We show that this new scheme has a simple and closed-form expression. In order to assess the benefits of such a detector for subpixel targets, we compare it to the popular algorithms using a real data experiment.

The paper is organized as follows. We first describe the replacement model and introduce the detection problem, in

section II. Section III is devoted to the computation of the one-step GLRT algorithm. This new detector is then compared to standard detectors through a real data benchmarking, in section IV. Finally concluding remarks end this paper in section V.

II. The replacement Model

As stated in the introduction, the replacement model writes [19]

$$\mathbf{y} = \alpha\mathbf{t} + (1-\alpha)\mathbf{b} \tag{1}$$

where

- $\mathbf{y}$ represents the spectral vector of the PUT, composed of N spectral-samples,
- $\mathbf{t}$ represents the target endmember
- $0 \leq \alpha \leq 1$ is the unknown target abundance, or fill factor,
- $\mathbf{b}$ is the background spectral signature, assumed to be Gaussian distributed with mean $\boldsymbol{\mu}$ and covariance matrix $\mathbf{R}$, which we denote as $\mathbf{b} \sim N(\boldsymbol{\mu}, \mathbf{R})$

Moreover, using the adjacent pixels, we assume that we have access to target-free data, $\mathbf{z}_k,\ k = 0..., (K-1)$, namely secondary data, supposed to be distributed as $\mathbf{z}_k \sim N(\boldsymbol{\mu}, \mathbf{R})$. The target signature $\mathbf{t}$ is assumed to be known from laboratory measurements [1] and will be considered as deterministic.
The detection problem aims at choosing between $H_0(\alpha = 0)$ and $H_1(\alpha \neq 0)$. As stated before, this detection problem is not standard, as the background power varies between the two hypotheses. Indeed, we should observe a noise decrease under H_1. This model is alike the detection problem derived in [20], but here the noise power and the target amplitude are linked together.

III. Exact (i.e. One-Step) GLRT

The direct GLRT consists in considering that the background characteristics (mean and covariance matrix) are not a-priori known. Thereby, the probability density of observing $\mathbf{y}$ under H_0 is shown to be

$$\begin{aligned} p_0 &= \frac{1}{\sqrt{(2\pi)^N|\mathbf{R}|}} e^{-\frac{1}{2}(\mathbf{y}-\boldsymbol{\mu})^T\mathbf{R}^{-1}(\mathbf{y}-\boldsymbol{\mu})} \\ &\times \prod_{k=0}^{K-1} \frac{1}{\sqrt{(2\pi)^N|\mathbf{R}|}} e^{-\frac{1}{2}(\mathbf{z}_k-\boldsymbol{\mu})^T\mathbf{R}^{-1}(\mathbf{z}_k-\boldsymbol{\mu})} \\ &= \frac{1}{[(2\pi)^N|\mathbf{R}|]^{\frac{K+1}{2}}} e^{-\frac{1}{2}\mathrm{Tr}\{\mathbf{R}^{-1}\boldsymbol{\Sigma}_0\}} \end{aligned}$$

where $\boldsymbol{\Sigma}_0 = (\mathbf{y}-\boldsymbol{\mu})(\mathbf{y}-\boldsymbol{\mu})^T + \sum_{k=0}^{K-1}(\mathbf{z}_k-\boldsymbol{\mu})(\mathbf{z}_k-\boldsymbol{\mu})^T$.

The mean and covariance matrix that maximize this Likelihood are shown to be respectively

$$\begin{aligned} \hat{\boldsymbol{\mu}}_0 &= \frac{K\bar{\mathbf{z}} + \mathbf{y}}{K+1} \\ \hat{\mathbf{R}}_0 &= \frac{1}{K+1}[\mathbf{Z}\mathbf{Z}^T - K\bar{\mathbf{z}}\bar{\mathbf{z}}^T + \frac{K}{K+1}(\mathbf{y}-\bar{\mathbf{z}})(\mathbf{y}-\bar{\mathbf{z}})^T] \end{aligned}$$

where $\mathbf{Z} = [\mathbf{z}_0 ... \mathbf{z}_{K-1}]$ and $\bar{\mathbf{z}} = \frac{1}{K}\sum_{k=0}^{K-1}\mathbf{z}_k$.

The likelihood under H_0 becomes

$$p_0 = \frac{1}{[(2\pi)^N|\hat{\mathbf{R}}_0|]^{\frac{K+1}{2}}} e^{-\frac{N(K+1)}{2}}$$

Similarly, the likelihood under H_1 is

$$\begin{aligned} p_1 &= \frac{1}{\sqrt{(2\pi)^N|(1-\alpha)^2\mathbf{R}|}} \\ &\times e^{-\frac{1}{2(1-\alpha)^2}(\mathbf{y}-\alpha\mathbf{t}-(1-\alpha)\boldsymbol{\mu})^T\mathbf{R}^{-1}(\mathbf{y}-\alpha\mathbf{t}-(1-\alpha)\boldsymbol{\mu})} \\ &\times \prod_{k=0}^{K-1} \frac{1}{\sqrt{(2\pi)^N|\mathbf{R}|}} e^{-\frac{1}{2}(\mathbf{z}_k-\boldsymbol{\mu})^T\mathbf{R}^{-1}(\mathbf{z}_k-\boldsymbol{\mu})} \\ &= \frac{1}{(1-\alpha)^N[(2\pi)^N|\mathbf{R}|]^{\frac{K+1}{2}}} e^{-\frac{1}{2}\mathrm{Tr}\{\mathbf{R}^{-1}\boldsymbol{\Sigma}_1\}} \end{aligned}$$

where

$$\begin{aligned} \boldsymbol{\Sigma}_1(\boldsymbol{\mu}) &= \sum_{k=0}^{K-1}(\mathbf{z}_k-\boldsymbol{\mu})(\mathbf{z}_k-\boldsymbol{\mu})^T \\ &+ \frac{[\mathbf{y}-\boldsymbol{\mu}-\alpha(\mathbf{t}-\boldsymbol{\mu})][\mathbf{y}-\boldsymbol{\mu}-\alpha(\mathbf{t}-\boldsymbol{\mu})]^T}{(1-\alpha)^2} \end{aligned}$$

Differentiating the likelihood with respect to $\boldsymbol{\mu}$ leads to

$$\hat{\boldsymbol{\mu}}_1 = \frac{1}{K+1}(K\bar{\mathbf{z}} + \tilde{\mathbf{y}})$$

with $\tilde{\mathbf{y}} = \frac{\mathbf{y}-\alpha\mathbf{t}}{1-\alpha}$. Then, the covariance matrix that maximizes p_1 is shown to be $\hat{\mathbf{R}}_1 = \frac{1}{K+1}\boldsymbol{\Sigma}_1(\hat{\boldsymbol{\mu}}_1)$, that can also be written as follows, after some straightforward calculations:

$$\hat{\mathbf{R}}_1 = \frac{1}{K+1}\left[\mathbf{Z}\mathbf{Z}^T - K\bar{\mathbf{z}}\bar{\mathbf{z}}^T + \frac{K}{K+1}(\tilde{\mathbf{y}}-\bar{\mathbf{z}})(\tilde{\mathbf{y}}-\bar{\mathbf{z}})^T\right]$$

The likelihood under H_1 becomes

$$p_1 = \frac{1}{(1-\alpha)^N[(2\pi)^N|\hat{\mathbf{R}}_1|]^{\frac{K+1}{2}}} e^{-\frac{N(K+1)}{2}}$$

The logarithm of this last expression writes

$$L_1 = \log(p_1) = -N\log(1-\alpha) - \frac{K+1}{2}\log(|\hat{\mathbf{R}}_1|) + \text{const.}$$

As we have

$$|\hat{\mathbf{R}}_1| = \frac{1}{(K+1)^N}|\mathbf{S}| \times [1 + \frac{K}{K+1}(\tilde{\mathbf{y}}-\bar{\mathbf{z}})^T\mathbf{S}^{-1}(\tilde{\mathbf{y}}-\bar{\mathbf{z}})]$$

where $\mathbf{S} = \mathbf{Z}\mathbf{Z}^T - K\bar{\mathbf{z}}\bar{\mathbf{z}}^T$, differentiating L_1 with respect to α, conducts to

$$\frac{\partial L_1}{\partial\alpha} = \frac{N}{1-\alpha} - \frac{K+1}{2}\frac{\frac{2K}{(K+1)(1-\alpha)^2}(\mathbf{y}-\mathbf{t})^T\mathbf{S}^{-1}(\tilde{\mathbf{y}}-\bar{\mathbf{z}})}{[1+\frac{K}{K+1}(\tilde{\mathbf{y}}-\bar{\mathbf{z}})^T\mathbf{S}^{-1}(\tilde{\mathbf{y}}-\bar{\mathbf{z}})]}$$

so that the Maximum Likelihood (ML) of α, that nulls this last expression, is the solution of the following second order equation

$$\begin{aligned} &(1-\alpha)^2 N[1 + \frac{K}{K+1}\bar{\mathbf{t}}^T\mathbf{S}^{-1}\bar{\mathbf{t}}] \\ &+ (1-\alpha)(\frac{2NK}{K+1} - K)[\boldsymbol{d}^T\mathbf{S}^{-1}\bar{\mathbf{t}}] \\ &+ (\frac{KN}{K+1} - K)[\boldsymbol{d}^T\mathbf{S}^{-1}\boldsymbol{d}] = 0 \end{aligned} \tag{2}$$

with $\bar{\mathbf{t}} = \mathbf{t} - \bar{\mathbf{z}}$ and $\boldsymbol{d} = (\mathbf{y} - \mathbf{t})$.
As we have $N < K + 1$, to ensure the invertibility of $\mathbf{S}$, the constant term is negative. Moreover, the coefficient of $(1-\alpha)^2$ is positive, so that the product of the two roots is negative. Hence, the only valid solution is the positive one, to ensure $\alpha \leq 1$.

Furthermore, considering that $|\hat{\mathbf{R}}_0| = \frac{1}{(K+1)^N}|\mathbf{S}|[1 + \frac{K}{K+1}\bar{\mathbf{y}}^T\mathbf{S}^{-1}\bar{\mathbf{y}}]$, the one-step GLRT writes as follows

$$T = \frac{|\hat{\mathbf{R}}_0|^{\frac{K+1}{2}}}{(1-\hat{\alpha})^N|\hat{\mathbf{R}}_1|^{\frac{K+1}{2}}} = \frac{(1 + \frac{K}{K+1}\bar{\mathbf{y}}^T\mathbf{S}^{-1}\bar{\mathbf{y}})^{\frac{K+1}{2}}}{(1-\hat{\alpha})^N[1 + \frac{K}{K+1}(\tilde{\mathbf{y}} - \bar{\mathbf{z}})^T\mathbf{S}^{-1}(\tilde{\mathbf{y}} - \bar{\mathbf{z}})]^{\frac{K+1}{2}}}$$

IV. Real Data Assesment

To assess the validity of previous derivations, we compare, in this last section, the performances of the proposed direct GLRT to two reference detectors, namely the MF and the FTMF. It has to be noticed that the MF has been developed for the standard additive model, where the noise level is the same under H_0 and H_1, whereas the FTMF has been developed for the replacement model, as stated in eq. (1).

For this benchmark we consider the "airborne Viareggio 2013 trial" [21], as we have access to the raw data measurements and a fully ground-truthed and documented scenario. Moreover, we also have access to calibrated ground targets to conduct a precise radiance to reflectance conversion. This pre-processing step is performed using the ELM method [15] [17], with the two proposed calibration targets, namely a black and white trap that can be seen on fig 1, respectively around the positions $[70, 330]$ and $[250, 150]$. This hyperspectral detection experiment was conducted in Viareggio (Italy), in May 2013, with an aircraft flying at 1200 meters heigh.

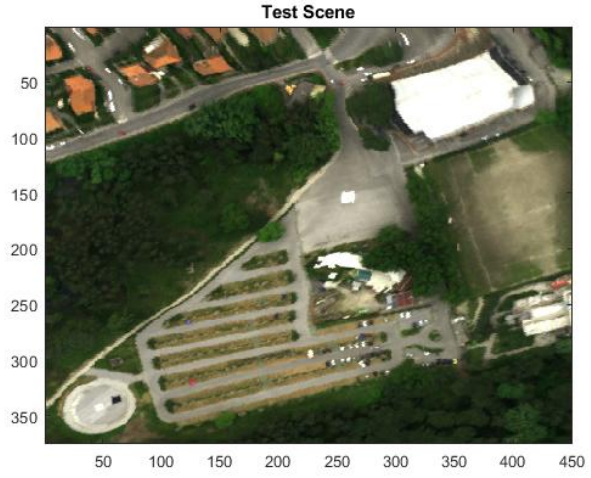

Fig. 1. Complete RGB view of the scene

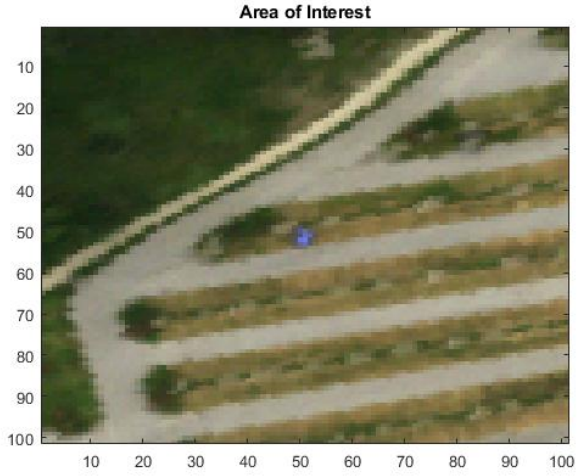

Fig. 2. RGB Zoom of the scene, centred in the target

The image size is $[450 \times 375]$ and each pixel is composed of $N = 511$ samples from the Visible Near InfraRed (VINR) band $(400 - 1000nm)$. The corresponding spatial ground resolution is about 0.6 meters. Different kinds of coloured panels as well as vehicles served as known and geo-referenced targets, as can be distinguished in the parking lot on fig 1. Each of these targets is characterized by a spectral signature, obtained from ground spectroradiometer measurements.

For the detection benchmarking we consider the vehicle referenced as V_1 in [21], as a target. It is a blue car that can be seen in the center of the zoomed image represented in fig. 2.

As stated before, a first processing step is performed to convert the raw radiance measurements into a reflectance map, using the ELM algorithm with a linear fitting transform. Then the number of spectral samples is reduced to 32 informative samples, in order to decrease the amount of necessary secondary data and to speed-up processing. For all the algorithms, the secondary pixels consist in a 9×9 guard window (as it is approximately the span of the target), a 11×11 pixels demeaning window (to estimate the background mean value), and a 15×15 pixels covariance matrix estimation window, all centred on the PUT, as specified in [22]. Thereby the total number of secondary pixels is $K = 144$, which is 4.5 times the size of the data. To finish with the covariance matrix estimation, we use Diagonal Loading (DL) to robustify the inversion step.

The detector outputs for the zoomed area around the target as represented on fig. 2, are plotted on figures 3, 4 and 5, for the MF, the FTMF and the proposed direct GLRT, respectively. We can first notice the better selectivity for both the two detectors matching the replacement model, as sorts of dashed lines are much more present on the MF output. These false targets correspond to parking-lot splitters that can be seen on fig. 2. This selectivity improvement was underlined in [18] where the FTMF was first derived. In order to evaluate more precisely

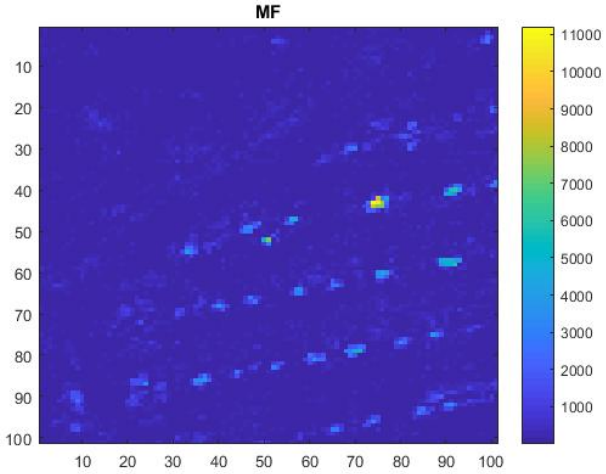

Fig. 3. MF output around the target

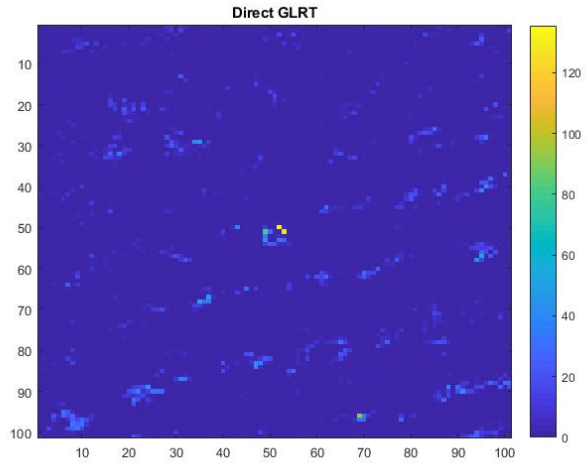

Fig. 5. Direct GLRT output around the target

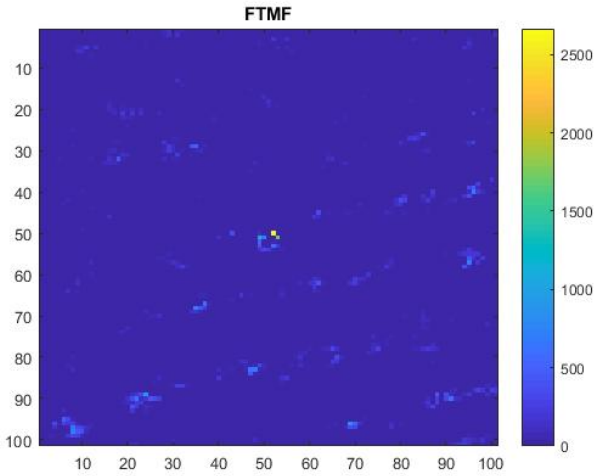

Fig. 4. FTMF output around the target

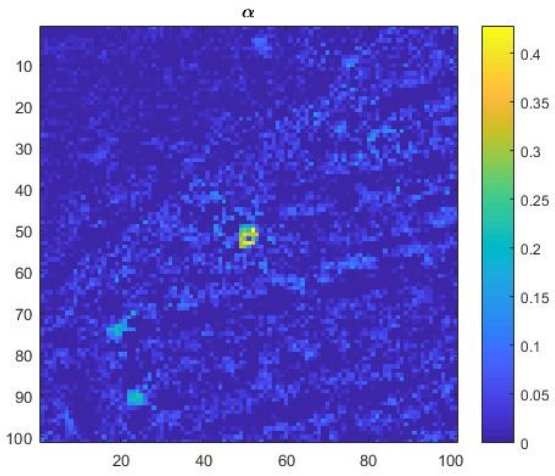

Fig. 6. Estimated Fill Factor

the performance of each detector, we compute the number of pixels, from the whole image, whose output is larger than the output for the actual target position. This figure can be seen as a false alarm number with an optimal thresholding. Using this criterion, the ranking of the 3 detectors of interest are represented in table I. As anticipated before, we can see the

MF	FTMF	Direct GLRT
13	4	0

TABLE I
FALSE ALARMS SCORE

superiority of the two detectors developed for the replacement model, with even a perfect detection, without any false alarm for the direct GLRT, presented in this paper. To finish with, we have also plotted the estimated value of the fill factor, $\hat{\alpha}$ computed from eq. (2), on fig. 6. We can observe that the fill factor obviously increases for the target position, with a maximum value of 40%, whereas it should be near 100%, if the target endmember was exactly the same as the reflectance measured in the PUT. This difference can be explained by target signature mismatches, as well as pre-processing errors or simply measurement noises.

V. CONCLUSIONS

In this communication, we consider the target detection problem for hyperspectral imaging. In spite of the existence of an underlying unitary constraint for reflectance images, the detectors exploiting this characteristic are rare. Thereby, we derived the exact GLRT for the model at hand, and show its superiority on a real data experiment.

REFERENCES

[1] D. G. Manolakis, R. B. Lockwood, and T. W. Cooley, *Hyperspectral Imaging Remote Sensing*. Cambridge University Press, 2016.

[2] E. Keith, H. Dan, O. William, J. Shridhar, B. Eustace, and L. Dereniak, "Hyperspectral imaging for astronomy and space surveillance," in *Proc. SPIE*, vol. 5159, January 2004.

[3] S. Michel, P. Gamet, and M.-J. Lefevre-Fonollosa, "Hypxim a hyperspectral satellite defined for science, security and defence users," in *Proceesings 3rd Workshop on Hyperspectral Image and Signal Processing: Evolution in Remote Sensing (WHISPERS)*, June 2011.

[4] H. Kwon and N. Nasrabadi, "Kernel rx-algorithm: a nonlinear anomaly detector for hyperspectral imagery," *IEEE Transactions Geoscience Remote Sensing*, vol. 43, no. 2, pp. 388–397, January 2005.

[5] E. M. Winter, M. Miller, C. Simi, A. Hill, T. Williams, D. Hampton, M. Wood, J. Zadnick, and M. Sviland, "Mine detection experiments using hyperspectral sensors," in *SPIE Int. Soc. Opt. Eng.*, Orlando, FL, United States, 21 September 2004.

[6] C. C. Funk, J. Theiler, D. A. Roberts, and C. C. Borel, "Clustering to improve matched filter detection of weak gas plumes in hyperspectral thermal imagery," *IEEE Transactions Geoscience Remote Sensing*, vol. 39, no. 7, pp. 1410–1420, July 2001.

[7] D.-W. Sun, *Hyperspectral Imaging for Food Quality Analysis and Control*. Elsevier, 2010.

[8] R. Koprowski, *Processing of Hyperspectral Medical Images, Applications in Dermatology Using Matlab*. Springer International Publishing, 2017.

[9] D. Manolakis and G. Shaw, "Detection algorithms for hyperspectral imaging applications," *IEEE Signal Processing Magazine*, pp. 29–43, January 2002.

[10] J. Settle, "On constrained energy minimization and the partial unmixing of multispectral images," *IEEE Transactions Geoscience Remote Sensing*, vol. 40, no. 3, pp. 718–721, March 2002.

[11] C. Chang, "Orthogonal subspace projection (osp) revisited: A comprehensive study and analysis," *IEEE Transactions Geoscience Remote Sensing*, vol. 43, no. 3, pp. 502–518, March 2005.

[12] E. Kelly, "An adaptive detection algorithm," *IEEE Transactions Aerospace Electronic Systems*, vol. 22, no. 2, pp. 115–127, March 1986.

[13] S. Kraut, L. L. Scharf, and L. T. McWhorter, "Adaptive subspace detectors," *IEEE Transactions Signal Processing*, vol. 49, no. 1, pp. 1–16, January 2001.

[14] E. F. Vermote, D. Tanre, J. L. Deuze, M. Herman, and J. J. Mercrett, "Second simulation of the satellite signal in the solar spectrum, 6s: an overview," *IEEE Transactions Geoscience Remote Sensing*, vol. 35, p. 675686, 1997.

[15] G. Ferrier, "Evaluation of apparent surface reflectance estimation methodologies," *International Journal of Remote Sensing*, vol. 16, pp. 2291–2297, 1995.

[16] T. Popp, "Correcting atmospheric masking to retrieve the spectral albedo of land surfaces from satellite measurements," *International Journal of Remote Sensing*, vol. 16, p. 34833508, 1995.

[17] G. M. Smith and E. J. Milton, "The use of the empirical line method to calibrate remotely sensed data to reflectance," *International Journal of Remote Sensing*, vol. 20, pp. 2653–2662, 1999.

[18] A. Schaum and A. Stocker, "Spectrally-selective target detection," in *Proceedings of ISSSR*, vol. 12, April 1997, pp. 2015–2018.

[19] D. Manolakis, R. Lockwood, T. Cooley, and J. Jacobson, "Is there a best hyperspectral detection algorithm?" in *Proc. of SPIE*, vol. 7334, 2009.

[20] F. Vincent, O. Besson, and C. Richard, "Matched subspace detection with hypothesis dependant noise power," *IEEE Transactions Signal Processing*, vol. 56, no. 11, pp. 5713–5718, November 2008.

[21] N. Acito, S. Matteoli, A. Rossi, M. Diani, and G. Corsini, "Hyperspectral airborne viareggio 2013 trial data collection for detection algorithm assessment," *IEEE Journal of Selected Topics in Applied Earth Observations and Remote Sensing*, vol. 9, no. 6, pp. 2356–2376, June 2016.

[22] S. Matteoli, M. Diani, and G. Corsini, "A tutorial overview of anomaly detection in hyperspectral i mages," *IEEE Aerospace Electronics Systems Magazine*, vol. 25, no. 7, pp. 5–27, July 2010.